Rapid Communications

Microscopic understanding of magnetic interactions in bilayer CrI_3

Seung Woo Jang, Min Yong Jeong, Hongkee Yoon, Siheon Ryee, and Myung Joon Han*
Department of Physics, Korea Advanced Institute of Science and Technology (KAIST), Daejeon 34141, Republic of Korea

(Received 1 November 2018; revised manuscript received 28 January 2019; published 28 March 2019)

We performed a detailed microscopic analysis of the interlayer magnetic couplings for bilayer CrI_3. As a first step toward understanding recent experimental observations and utilizing them for device applications, we estimated the magnetic force response as well as total energy. Various van der Waals functionals unequivocally point to the ferromagnetic ground state for the low-temperature structured bilayer CrI_3 which is further confirmed independently by magnetic force response calculations. The calculated orbital-dependent magnetic forces clearly show that the e_g-t_{2g} interaction is the key to stabilize this ferromagnetic order. By suppressing this ferromagnetic interaction and enhancing antiferromagnetic orbital channels of e_g-e_g and t_{2g}-t_{2g}, one can realize the desirable antiferromagnetic order. We showed that high-temperature monoclinic stacking can be the case. Our results provide unique information and insight into understanding the magnetism of multilayer CrI_3, paving the way to utilize it for applications.

DOI: 10.1103/PhysRevMaterials.3.031001

Recently, magnetism in two-dimensional (2D) van der Waals (vdW) materials has attracted great attention [1–20]. It is not just due to its novelty from a fundamental physics point of view, but also to its great potential for device applications. Importantly, however, understanding the microscopic nature of those magnetic interactions is far from complete, posing an outstanding challenge for theoretical material science. The difficulty is partly attributed to there being no well-established exchange-correlation functional for describing the vdW interaction. Although there are several promising functionals now available [21–32], a reliable description of this weak interaction is still quite challenging for first-principles simulations. Another difficulty is related to the lack of a conventional physical "picture" to describe the magnetic interactions in these materials such as a superexchange and double-exchange model for typical ionic solids. Without such an intuitive picture, a clear understanding of the observed phenomena and utilizing them for device applications are severely hampered.

An outstanding example to demonstrate this type of challenge is CrI_3. Just after the first realization of a CrI_3 monolayer [9], this magnetic insulating 2D material has generated great research interest [9–20]. While monolayer ferromagnetism is well reproduced by first-principles calculations [33–37], understanding the multilayer systems remains quite elusive. A recent magneto-optical Kerr effect (MOKE) measurement of bilayer CrI_3 shows a vanishing Kerr rotation which indicates interlayer antiferromagnetic (AFM) coupling by excluding ferromagnetism [9]. AFM order is further confirmed by magnetophotoluminescence (PL) [11], reflective magnetic circular dichroism (RMCD), and transport measurements [12,14–16,18]. On the contrary, however, first-principles calculations report that ferromagnetic (FM) spin order with a low-temperature (LT) structure is energetically most favorable [38,39].

In this Rapid Communication, we investigate the magnetic interactions of bilayer CrI_3. First, we perform total energy calculations with various forms of exchange-correlation functionals supported by the state-of-the-art constrained random phase approximation (cRPA) technique. It is found that FM interlayer coupling is always favorable in LT stacking, which provides a stronger indication of FM order in this structure. Further, we perform a magnetic force response calculation which can directly measure the spin-spin interaction independent of the total energy values. The calculated magnetic responses unequivocally point to FM interlayer coupling, which is another strong evidence. In order to unveil the microscopic origin of interlayer couplings, we investigate the orbitally decomposed magnetic interactions using our recent implementation [40]. Surprisingly, Cr-e_g orbitals are found to play an important role. Our calculations clearly show that second-neighbor e_g-t_{2g} interactions are the main source of FM order in LT-structured bilayer CrI_3. This coupling is significantly suppressed and becomes comparable with the AFM e_g-e_g interaction in high-temperature (HT) structures. Our analysis provides detailed information and insight, which pave the way toward understanding the fascinating phenomena reported in this material [9,11] and utilizing them for device applications [12–19].

The total energy calculations with different vdW functionals were carried out with the VASP code [41]. We considered many different exchange-correlation functionals including the local density approximation (LDA) [42,43], Perdew-Burke-Ernzerhof (PBE) [44], PBEsol [45], D2 [21], D3 (Grimme), D3 (BJ) [22,23], Tkatchenko-Scheffler (TS) [24], MBD@rsSCS [25,26], dDsC [27,28], vdW-DF-optB86b [29–31], and vdW-DF2-rPW86 [32]. The 600-eV energy cutoff and $9 \times 9 \times 1$ **k** points were used in the first Brillouin zone for all the functionals. We found these numerical settings are enough to achieve the desirable accuracy. Atomic positions were relaxed with a force criterion of 1 meV/Å and the lattice constants fixed to the experimental values: $a = b = 6.867$ Å

*mj.han@kaist.ac.kr

for rhombohedral LT and $a = b = 6.863$ Å for monoclinic HT stackings [46]. We also found that the magnetic ground state is not changed when using optimized lattice constants. We took a vacuum distance of ∼20 Å which is found to be large enough to simulate the experimental situation. For DFT + U (density functional theory plus U) method [47], we used the so-called fully localized limit (FLL) version of DFT + U based on charge density [48,49]. It is found that spin-orbit coupling does not change the magnetic ground state, which is consistent with the previous calculation by Sivadas *et al.* [50]. For the magnetic force theory (MFT) calculation [40,51–53], we used the OPENMX software package [54,55] which is based on the linear combination of pseudoatomic orbitals (LCPAO) formalism. An $8 \times 8 \times 1$ **k** mesh was used for the MFT calculation. The D3 method of Grimme *et al.* was used for the vdW correction [22] in this process since it best reproduces the lattice constants and the cell volume for bulk CrI_3. For the estimation of interaction parameters, the constrained random phase approximation (cRPA) [56,57] was performed with the ECALJ package [58]. We used the so-called d-dp model [59,60] as derived by the maximally localized Wannier function technique [61].

While many of theoretical studies have been devoted to bulk and monolayer CrI_3 [33–37,46,62–66], the interlayer interaction of bilayers or multilayers is largely unexplored. Three first-principles investigations have been reported quite recently which focus on the stacking patterns to understand the interlayer coupling [17,38,39]. The total energy calculations based on the generalized gradient approximation (GGA) or GGA + U with a certain type of vdW correction show that FM interlayer spin order with a LT (rhombohedral) structure is energetically most favorable for bilayer CrI_3, in contrast to experimental observations [17,38,39].

Let us start by noting that the computation studies are limited to a couple of vdW functional recipes, namely, (so-called) svdW-DF [17], vdW-DF-optB86b + U [38], and PBE-D2 [39]. Since the universal vdW functional within the density functional framework is not yet well established, it is strongly required to confirm whether this is a physically reasonable solution, not an artifact, especially considering the inconsistency with experiments. Further, this material CrI_3 is known to be a Mott insulator [46] for which the conventional LDA or GGA functional does not give a reasonable electronic structure. This is the reason why several recent studies adopted LDA/GGA + U functionals [38,63,67]. While DFT + U is certainly the better choice for Mott insulators, its final result critically depends on the choice of "interaction parameters" such as the Hubbard U and Hund J_H. Indeed, a previous study by Jiang *et al.* shows that the spin ground state of HT-phase bilayer CrI_3 changes from FM to AFM at around $U = 2.5$ eV [38].

Here, we first estimate the interaction parameters based on the most advanced scheme, namely, cRPA [56,57], which is computationally demanding but known to be quite reliable [68–72]. The calculated on-site Coulomb repulsion $U = 2.0$ eV for the bulk CrI_3 and $U = 2.9$ eV for the monolayer. The Hund interaction is found to be $J_H = 0.7$ eV for both the bulk and monolayer. It is noted that the on-site electron correlation U is significantly enhanced by ∼30% when the system dimension is reduced. This value is used for our bilayer calculations.

Now we investigate the total energy profile to confirm the magnetic ground state of the LT structure. We consider most of the available vdW functionals including eight different correction types. The results are summarized in Fig. 1. It is clearly shown that the interlayer AFM order is not stabilized in LT stacking; see the blue diamonds in Fig. 1. For all of the functional choices, the calculated total energies of AFM order are larger than those of FM by more than ∼0.78 meV per formula unit (f.u.), except for PBEsol (see Fig. 1). Our result is strong evidence that the ground state of bilayer CrI_3 is FM in LT stacking.

As discussed in previous studies, AFM interlayer coupling is important for device applications [11–19]. To explore this possibility and to understand the fascinating recent experimental observations such as voltage-controlled magnetism [12–14] and giant magnetoresistance (GMR) [15–19], a key first step is to have a microscopic picture of the interlayer

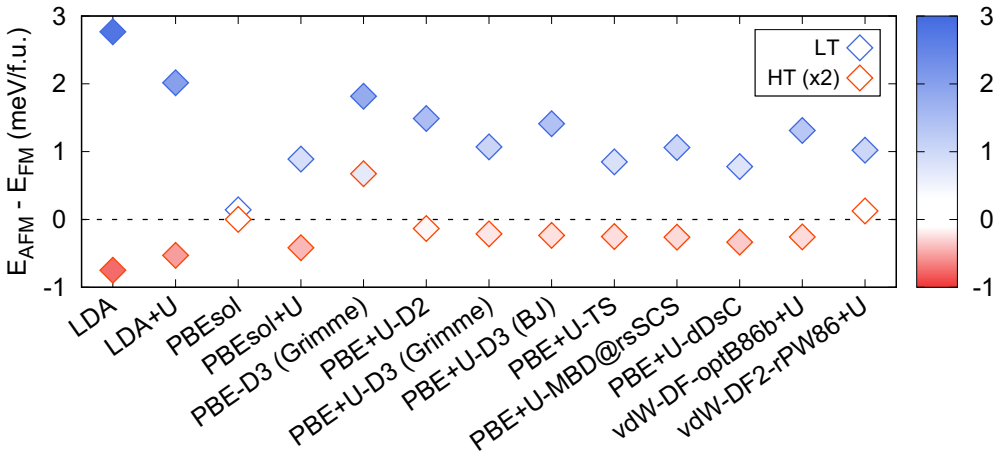

FIG. 1. The calculated total energy difference between layered AFM and FM with various functionals. E_{FM} and E_{AFM} denote the calculated total energy for the interlayer FM and AFM phase, respectively. The blue and red symbols represent the results of LT and HT stacking, respectively (see the inset). The solid colors represent the calculated value of energy difference (see the color bar). For a clear presentation, the calculated values for HT stacking have been multiplied by 2.

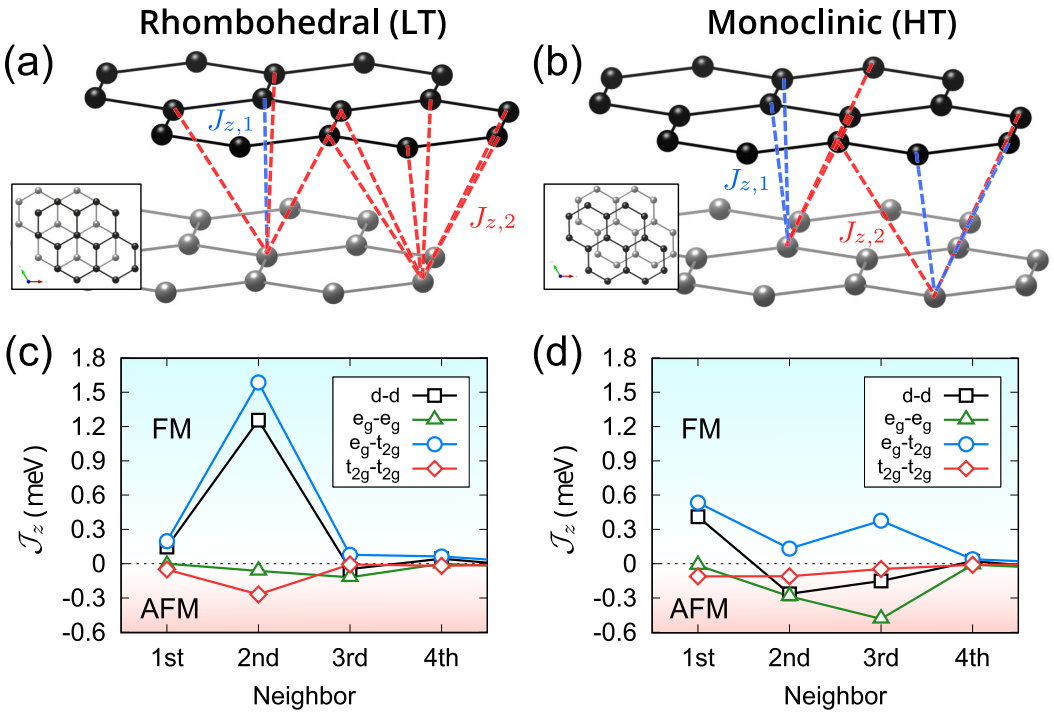

FIG. 2. (a), (b) The schematic picture of interlayer magnetic interactions in bilayer CrI_3 of (a) LT rhombohedral and (b) HT monoclinic structure. The first ($J_{z,1}$) and the second neighboring interlayer couplings ($J_{z,2}$) are represented by blue and red colors, respectively. The black and gray atoms represent Cr. Insets of (a) and (b) represent the top view of each stacking. (c), (d) The calculated $\mathcal{J}_z$ values as a function of neighboring distance. The positive and negative values correspond to FM and AFM interactions, respectively. The interactions through each orbital pair channel are represented by different colors and symbols as denoted in the inset of (d). The black lines with squares refer to the total d orbital interactions which correspond to the sum of e_g-e_g, e_g-t_{2g}, and t_{2g}-t_{2g} interactions.

interactions. Here, we note that the conventional interaction model such as superexchange is not relevant to this case of vdW materials as second-order hopping does not connect even the first neighboring Cr sites. Thus, a simple-model-based approach can hardly be successful, and a first-principles-based simulation is desirable. With this motivation, we performed the MFT calculations in which the magnetic interaction J is calculated as a response to the small angle tilting of spin rotations [40,51–53].

Our results of MFT are summarized in Fig. 2 where the nth neighbor out-of-plane interaction $\mathcal{J}_{z,n}$ is defined as the sum of all pairs of $J_{z,n}$ reflecting the corresponding coordination number. For the LT-stacked bilayer CrI_3, the calculated interlayer coupling $\mathcal{J}_z$ is FM; see the black line with squares in Fig. 2(c). The nearest neighbor $\mathcal{J}_{z,1}$ and the second neighbor $\mathcal{J}_{z,2}$ are both FM [73] whereas the longer-range interlayer interactions ($\mathcal{J}_{z,n\geqslant 3}$) are negligibly small. This is another meaningful confirmation that AFM order is not stabilized in LT stacking. It is important to note that the MFT calculation does not rely on total energy information, but just utilizes eigenfunctions and eigenvalues [40,51–53]. Indeed, when we calculated $\mathcal{J}_z$ values based on the AFM solution of the LT structure (which is not the ground state), the response function favors the spin flip, indicative of a FM ground state. Our MFT results provide an additional independent confirmation of FM interlayer coupling in LT structures.

In order to obtain further insights, we calculate orbitally decomposed magnetic interactions, which are unique and useful features of MFT. As shown in Fig. 2(c), the dominant contribution comes from FM e_g-t_{2g} channels (see the blue line with circles). The e_g-e_g and t_{2g}-t_{2g} orbital interactions are AFM but significantly weaker. This detailed microscopic information provides unique insights into understanding the magnetism of this material. It is remarkable that e_g orbitals play an important role which should be magnetically inactive in the pure ionic picture of Cr^{3+}. Due to the hybridization with I-p orbitals, the e_g states carry sizable moments as shown in Table I. This feature has not been properly recognized before [38,39] and it demonstrates an intriguing nature of vdW magnetic materials distinctive from the typical ionic Mott insulators.

One important implication of our orbital-decomposed $\mathcal{J}$ results is that, if one can suppress the e_g-t_{2g} interaction and enhance e_g-e_g and/or t_{2g}-t_{2g}, AFM order can be stabilized, which is desirable for many purposes [12–19]. As one

TABLE I. The calculated orbital-resolved electron occupations and magnetic moments for HT stacking. The ↑ and ↓ denote the up and down spins, respectively. The e_g and t_{2g} states are defined in each atomic local axis.

		$N_\uparrow$	$N_\downarrow$	M
Cr	e_g	1.10	0.51	0.59
	t_{2g}	2.85	0.15	2.70
	d	3.95	0.66	3.29
I	p	2.61	2.75	−0.14

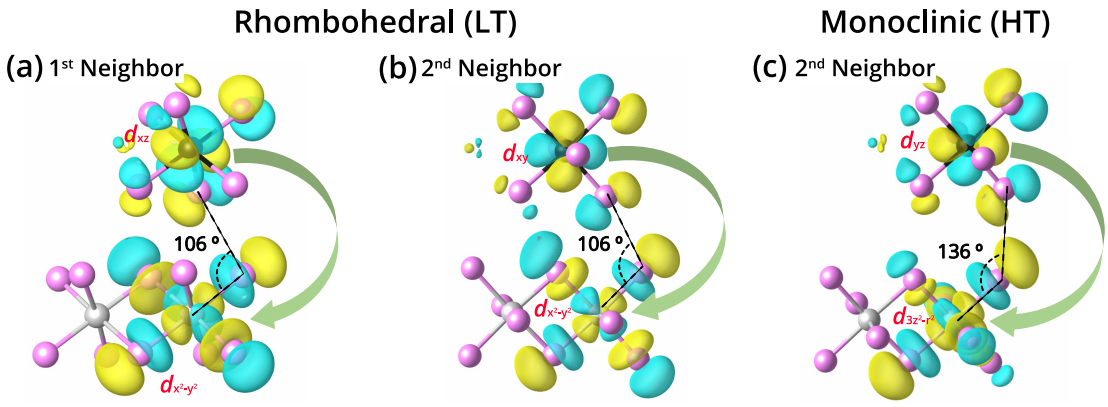

FIG. 3. Maximally localized Wannier orbitals for (a), (b) LT and (c) HT stacking. The green arrows highlight the e_g-t_{2g} magnetic interaction for the first neighbor in (a) and the second neighbor pairs in (b) and (c).

example of this, we calculated the HT-stacked monoclinic bilayer [see Fig. 2(b)], and the results are presented in Fig. 2(d). The HT structure of bulk CrI_3 is specified by the space group $C2/m$ and the LT structure by $R\bar{3}$. Importantly, the different stacking leads to different numbers of magnetic couplings. For bilayer CrI_3, HT stacking has four first-neighbor and four second-neighbor couplings whereas LT stacking has one nearest and nine next-nearest neighbors. Due to the change of hopping routes (to be discussed further below) as well as the different numbers of neighboring sites, the orbital interaction profile is notably different from that of the LT structure. While the e_g-t_{2g} interactions $\mathcal{J}_z^{e_g\text{-}t_{2g}}$ are still FM, the second neighbor $\mathcal{J}_{z,2}^{e_g\text{-}t_{2g}}$ becomes significantly weaker. As a result, the total $\mathcal{J}_{z,2}$ becomes AFM in the HT structure. It is also noted that the third neighbor $\mathcal{J}_{z,3}$ is sizable and AFM, which is largely due to the enhanced AFM coupling $\mathcal{J}_{z,3}^{e_g\text{-}e_g}$. The total sum of magnetic interactions in the HT phase is AFM being consistent with the calculated total energy results shown in Fig. 1; see the red diamonds, which are mostly negative values [74]. Microscopically, the magnetic interaction and the ground-state spin order of bilayer CrI_3 can be understood from the competition and the cooperation of FM $\mathcal{J}^{e_g\text{-}t_{2g}}$, AFM $\mathcal{J}^{e_g\text{-}e_g}$, and AFM $\mathcal{J}^{t_{2g}\text{-}t_{2g}}$ couplings.

The significantly reduced $\mathcal{J}_{z,2}^{e_g\text{-}t_{2g}}$ of the HT phase is mainly attributed to a bond angle change, as clearly seen in the analysis of maximally localized Wannier orbitals. Figures 3(a) and 3(b) show that the main interaction path for $\mathcal{J}_{z,2}^{e_g\text{-}t_{2g}}$ in the LT structure is the hopping between Cr-e_g and t_{2g} through the e_g-I_p σ, I_p-I_p π, and I_p-t_{2g} π bondings, which is clearly beyond the conventional superexchange process. This analysis also shows the reason why the interlayer magnetic interaction is small ($\sim$0.1 meV): Due to the two successive hopping required, the magnetic interaction of this vdW 2D material is much weaker than the usual superexchange scale. One can further understand why this interaction $\mathcal{J}_{z,2}^{e_g\text{-}t_{2g}}$ is reduced in the HT phase. The calculated maximally localized Wannier functions for the HT phase are presented in Fig. 3(c). The second neighbor $\mathcal{J}_{z,2}^{e_g\text{-}t_{2g}}$ is reduced owing to the bonding angle enlarged from 106° (LT phase) to 136° (HT phase) which leads to the weaker I_p-I_p π hopping [see Fig. 3(c)]. This effect gives rise to $J_{z,2}^{e_g\text{-}t_{2g}} \sim 0.02$ meV for the HT structure which is $\sim$22% of the LT value [75].

To summarize, we investigated the magnetic interactions of bilayer CrI_3 from two different points of views, namely, energetics and magnetic response. Both approaches point to the same conclusion, that the interlayer AFM order could not be stabilized in the LT-structured bilayer. Further, by analyzing the orbital-resolved magnetic couplings, we found that the second-neighbor e_g-t_{2g} interaction plays the key role in stabilizing the FM order. This interaction can effectively be suppressed and becomes comparable with AFM e_g-e_g interactions in HT stacking, whereby the interlayer AFM order is stabilized. Our results provide unique information and insight into understanding the magnetism of bilayer CrI_3, paving the way to utilize it for applications.

Note added. Recently, we became aware of a related study [50] which contains a qualitative discussion of stacking-dependent magnetism based on the calculated total energies.

This work was supported by the Basic Science Research Program through the National Research Foundation of Korea (NRF) funded by the Ministry of Education (2018R1A2B2005204) and Creative Materials Discovery Program through the NRF funded by the Ministry of Science and ICT (2018M3D1A1058754). The computing resource was partly supported by the Computing System for Research in Kyushu University.

[1] X. Wang, K. Du, Y. Y. F. Liu, P. Hu, J. Zhang, Q. Zhang, M. H. S. Owen, X. Lu, C. K. Gan, P. Sengupta, C. Kloc, and Q. Xiong, 2D Mater. **3**, 031009 (2016).

[2] Y. Tian, M. J. Gray, H. Ji, R. J. Cava, and K. S. Burch, 2D Mater. **3**, 025035 (2016).

[3] J.-U. Lee, S. Lee, J. H. Ryoo, S. Kang, T. Y. Kim, P. Kim, C.-H. Park, J.-G. Park, and H. Cheong, Nano Lett. **16**, 7433 (2016).

[4] C. Gong, L. Li, Z. Li, H. Ji, A. Stern, Y. Xia, T. Cao, W. Bao, C. Wang, Y. Wang, Z. Q. Qiu, R. J. Cava, S. G. Louie, J. Xia, and X. Zhang, Nature (London) **546**, 265 (2017).

[5] M. Bonilla, S. Kolekar, Y. Ma, H. C. Diaz, V. Kalappattil, R. Das, T. Eggers, H. R. Gutierrez, M.-H. Phan, and M. Batzill, Nat. Nanotechnol. **13**, 289 (2018).

[6] S. Y. Kim, T. Y. Kim, L. J. Sandilands, S. Sinn, M.-C. Lee, J. Son, S. Lee, K.-Y. Choi, W. Kim, B.-G. Park, C. Jeon, H.-D. Kim, C.-H. Park, J.-G. Park, S. J. Moon, and T. W. Noh, Phys. Rev. Lett. **120**, 136402 (2018).

[7] Z. Wang, T. Zhang, M. Ding, B. Dong, Y. Li, M. Chen, X. Li, J. Huang, H. Wang, X. Zhao, Y. Li, D. Li, C. Jia, L. Sun, H. Guo, Y. Ye, D. Sun, Y. Chen, T. Yang, J. Zhang *et al.*, Nat. Nanotechnol. **13**, 554 (2018).

[8] Z. Fei, B. Huang, P. Malinowski, W. Wang, T. Song, J. Sanchez, W. Yao, D. Xiao, X. Zhu, A. F. May, W. Wu, D. H. Cobden, J.-H. Chu, and X. Xu, Nat. Mater. **17**, 778 (2018).

[9] B. Huang, G. Clark, E. Navarro-Moratalla, D. R. Klein, R. Cheng, K. L. Seyler, D. Zhong, E. Schmidgall, M. A. McGuire, D. H. Cobden, W. Yao, D. Xiao, P. Jarillo-Herrero, and X. Xu, Nature (London) **546**, 270 (2017).

[10] D. Zhong, K. L. Seyler, X. Linpeng, R. Cheng, N. Sivadas, B. Huang, E. Schmidgall, T. Taniguchi, K. Watanabe, M. A. McGuire, W. Yao, D. Xiao, K.-M. C. Fu, and X. Xu, Sci. Adv. **3**, e1603113 (2017).

[11] K. L. Seyler, D. Zhong, D. R. Klein, S. Gao, X. Zhang, B. Huang, E. Navarro-Moratalla, L. Yang, D. H. Cobden, M. A. McGuire, W. Yao, D. Xiao, P. Jarillo-Herrero, and X. Xu, Nat. Phys. **14**, 277 (2018).

[12] S. Jiang, J. Shan, and K. F. Mak, Nat. Mater. **17**, 406 (2018).

[13] S. Jiang, L. Li, Z. Wang, K. F. Mak, and J. Shan, Nat. Nanotechnol. **13**, 549 (2018).

[14] B. Huang, G. Clark, D. R. Klein, D. MacNeill, E. Navarro-Moratalla, K. L. Seyler, N. Wilson, M. A. McGuire, D. H. Cobden, D. Xiao, W. Yao, P. Jarillo-Herrero, and X. Xu, Nat. Nanotechnol. **13**, 544 (2018).

[15] T. Song, X. Cai, M. W.-Y. Tu, X. Zhang, B. Huang, N. P. Wilson, K. L. Seyler, L. Zhu, T. Taniguchi, K. Watanabe, M. A. McGuire, D. H. Cobden, D. Xiao, W. Yao, and X. Xu, Science **360**, 1214 (2018).

[16] D. R. Klein, D. MacNeill, J. L. Lado, D. Soriano, E. Navarro-Moratalla, K. Watanabe, T. Taniguchi, S. Manni, P. Canfield, J. Fernández-Rossier, and P. Jarillo-Herrero, Science **360**, 1218 (2018).

[17] Z. Wang, I. Gutiérrez-Lezama, N. Ubrig, M. Kroner, M. Gibertini, T. Taniguchi, K. Watanabe, A. Imamoğlu, E. Giannini, and A. F. Morpurgo, Nat. Commun. **9**, 2516 (2018).

[18] H. H. Kim, B. Yang, T. Patel, F. Sfigakis, C. Li, S. Tian, H. Lei, and A. W. Tsen, Nano Lett. **18**, 4885 (2018).

[19] T. Song, M. W.-Y. Tu, C. Carnahan, X. Cai, T. Taniguchi, K. Watanabe, M. A. McGuire, D. H. Cobden, D. Xiao, W. Yao, and X. Xu, Nano Lett. **19**, 915 (2019).

[20] C. Cardoso, D. Soriano, N. A. García-Martínez, and J. Fernández-Rossier, Phys. Rev. Lett. **121**, 067701 (2018).

[21] S. Grimme, J. Comput. Chem. **27**, 1787 (2006).

[22] S. Grimme, J. Antony, S. Ehrlich, and H. Krieg, J. Chem. Phys. **132**, 154104 (2010).

[23] S. Grimme, S. Ehrlich, and L. Goerigk, J. Comput. Chem. **32**, 1456 (2011).

[24] A. Tkatchenko and M. Scheffler, Phys. Rev. Lett. **102**, 073005 (2009).

[25] A. Tkatchenko, R. A. DiStasio, R. Car, and M. Scheffler, Phys. Rev. Lett. **108**, 236402 (2012).

[26] A. Ambrosetti, A. M. Reilly, R. A. DiStasio, and A. Tkatchenko, J. Chem. Phys. **140**, 18A508 (2014).

[27] S. N. Steinmann and C. Corminboeuf, J. Chem. Theory Comput. **7**, 3567 (2011).

[28] S. N. Steinmann and C. Corminboeuf, J. Chem. Phys. **134**, 044117 (2011).

[29] M. Dion, H. Rydberg, E. Schröder, D. C. Langreth, and B. I. Lundqvist, Phys. Rev. Lett. **92**, 246401 (2004).

[30] G. Román-Pérez and J. M. Soler, Phys. Rev. Lett. **103**, 096102 (2009).

[31] J. Klimeš, D. R. Bowler, and A. Michaelides, Phys. Rev. B **83**, 195131 (2011).

[32] K. Lee, É. D. Murray, L. Kong, B. I. Lundqvist, and D. C. Langreth, Phys. Rev. B **82**, 081101(R) (2010).

[33] H. Wang, V. Eyert, and U. Schwingenschlögl, J. Phys.: Condens. Matter **23**, 116003 (2011).

[34] N. Sivadas, M. W. Daniels, R. H. Swendsen, S. Okamoto, and D. Xiao, Phys. Rev. B **91**, 235425 (2015).

[35] P. Jiang, L. Li, Z. Liao, Y. X. Zhao, and Z. Zhong, Nano Lett. **18**, 3844 (2018).

[36] J. L. Lado and J. Fernández-Rossier, 2D Mater. **4**, 035002 (2017).

[37] F. Zheng, J. Zhao, Z. Liu, M. Li, M. Zhou, S. Zhang, and P. Zhang, Nanoscale **10**, 14298 (2018).

[38] P. Jiang, C. Wang, D. Chen, Z. Zhong, Z. Yuan, Z.-Y. Lu, and W. Ji, arXiv:1806.09274.

[39] D. Soriano, C. Cardoso, and J. Fernández-Rossier, arXiv:1807.00357.

[40] H. Yoon, T. J. Kim, J.-H. Sim, S. W. Jang, T. Ozaki, and M. J. Han, Phys. Rev. B **97**, 125132 (2018).

[41] G. Kresse and D. Joubert, Phys. Rev. B **59**, 1758 (1999).

[42] D. M. Ceperley and B. J. Alder, Phys. Rev. Lett. **45**, 566 (1980).

[43] J. P. Perdew and A. Zunger, Phys. Rev. B **23**, 5048 (1981).

[44] J. P. Perdew, K. Burke, and M. Ernzerhof, Phys. Rev. Lett. **77**, 3865 (1996).

[45] J. P. Perdew, A. Ruzsinszky, G. I. Csonka, O. A. Vydrov, G. E. Scuseria, L. A. Constantin, X. Zhou, and K. Burke, Phys. Rev. Lett. **100**, 136406 (2008).

[46] M. A. McGuire, H. Dixit, V. R. Cooper, and B. C. Sales, Chem. Mater. **27**, 612 (2015).

[47] V. I. Anisimov, F. Aryasetiawan, and A. Lichtenstein, J. Phys.: Condens. Matter **9**, 767 (1997).

[48] V. I. Anisimov, I. V. Solovyev, M. A. Korotin, M. T. Czyżyk, and G. A. Sawatzky, Phys. Rev. B **48**, 16929 (1993).

[49] S. Ryee and M. J. Han, Sci. Rep. **8**, 9559 (2018).

[50] N. Sivadas, S. Okamoto, X. Xu, C. J. Fennie, and D. Xiao, Nano Lett. **18**, 7658 (2018).

[51] T. Oguchi, K. Terakura, and A. R. Williams, Phys. Rev. B **28**, 6443 (1983).

[52] A. I. Liechtenstein, M. I. Katsnelson, V. P. Antropov, and V. A. Gubanov, J. Magn. Magn. Mater. **67**, 65 (1987).

[53] M. J. Han, T. Ozaki, and J. Yu, Phys. Rev. B **70**, 184421 (2004).

[54] www.openmx-square.org.

[55] T. Ozaki, Phys. Rev. B **67**, 155108 (2003).

[56] F. Aryasetiawan, M. Imada, A. Georges, G. Kotliar, S. Biermann, and A. I. Lichtenstein, Phys. Rev. B **70**, 195104 (2004).

[57] E. Şaşıoğlu, C. Friedrich, and S. Blügel, Phys. Rev. B **83**, 121101(R) (2011).

[58] https://github.com/tkotani/ecalj/.

[59] T. Miyake, L. Pourovskii, V. Vildosola, S. Biermann, and A. Georges, J. Phys. Soc. Jpn. **77**, 99 (2008).
[60] L. Vaugier, H. Jiang, and S. Biermann, Phys. Rev. B **86**, 165105 (2012).
[61] N. Marzari, A. A. Mostofi, J. R. Yates, I. Souza, and D. Vanderbilt, Rev. Mod. Phys. **84**, 1419 (2012).
[62] W.-B. Zhang, Q. Qu, P. Zhu, and C.-H. Lam, J. Mater. Chem. C **3**, 12457 (2015).
[63] J. Liu, Q. Sun, Y. Kawazoe, and P. Jena, Phys. Chem. Chem. Phys. **18**, 8777 (2016).
[64] D. T. Larson and E. Kaxiras, Phys. Rev. B **98**, 085406 (2018).
[65] L. Webster, L. Liang, and J.-A. Yan, Phys. Chem. Chem. Phys. **20**, 23546 (2018).
[66] S. Djurdjić-Mijin, A. Šolajić, J. Pešić, M. Šćepanović, Y. Liu, A. Baum, C. Petrovic, N. Lazarević, and Z. V. Popović, Phys. Rev. B **98**, 104307 (2018).
[67] T. Olsen, Phys. Rev. B **96**, 125143 (2017).
[68] T. O. Wehling, E. Şaşıoğlu, C. Friedrich, A. I. Lichtenstein, M. I. Katsnelson, and S. Blügel, Phys. Rev. Lett. **106**, 236805 (2011).
[69] P. Werner, M. Casula, T. Miyake, F. Aryasetiawan, A. J. Millis, and S. Biermann, Nat. Phys. **8**, 331 (2012).
[70] Y. Yamaji, Y. Nomura, M. Kurita, R. Arita, and M. Imada, Phys. Rev. Lett. **113**, 107201 (2014).
[71] S. W. Jang, H. Sakakibara, H. Kino, T. Kotani, K. Kuroki, and M. J. Han, Sci. Rep. **6**, 33397 (2016).
[72] S. W. Jang, S. Ryee, H. Yoon, and M. J. Han, Phys. Rev. B **98**, 125126 (2018).
[73] The largest value of $\mathcal{J}_{z,2}$ is partly attributed to the larger numbers of pairs. While $J_{z,1} \approx J_{z,2}$ per bonding (the difference is $\sim$0.01 meV), the number of second neighbors is nine and that of the first neighbor is one.
[74] It should be noted that the calculated total energy of the AFM HT structure is greater than that of the FM LT structure by 0.2–6.6 meV/f.u. in our calculations. While the energy barrier between these two phases might be overcome in a certain stage of the experimental processes, it still remains unclear if the HT structure was indeed realized in previous experiments.
[75] The result of Fig. 2 also reflects the number of second neighbors, which are four and 9 in HT- and LT-structured phases, respectively.